

XAFS study of interchain and intrachain order in $\text{Se}_{1-x}\text{Te}_x$ glasses: Nearest neighbors

M. Majid

*Laboratoire de Chimie Minérale, Inorganique, et Bioinorganique, Centre Pharmaceutique Châtenay-Malabry,
Université Paris-Sud, 92296 Châtenay-Malabry, France*

S. Bénazeth

*Laboratoire de Chimie Minérale, Inorganique, et Bioinorganique, Centre Pharmaceutique Châtenay-Malabry,
Université Paris-Sud, 92296 Châtenay-Malabry, France
and LURE, Université Paris-Sud, Bâtiment 209D, 91405 Orsay, France*

C. Souleau

*Laboratoire de Chimie Minérale, Inorganique, et Bioinorganique, Centre Pharmaceutique Châtenay-Malabry,
Université Paris-Sud, 92296 Châtenay-Malabry, France*

J. Purans*

Institute of Solid State Physics, University of Latvia, LV-1063 Riga, Latvia

(Received 31 March 1998)

XAFS measurements (LURE and NSLS) of $\text{Se}_{1-x}\text{Te}_x$ glasses have been carried out on both the Se and Te *K* edges at low and room temperatures. Using a multishell best-fit analysis procedure, we have reconstructed the Se and Te local environment: first-shell intrachain nearest neighbors (Se- Se_1 , Se- Te_1 , Te- Se_1 , and Te- Te_1). We conclude that the intrachain chemical order (preferential of Se-Te pairs) increases with Te content in the glasses. On the other hand, we suggest a random distribution of Se and Te atoms between the chains. The thermal disorder dominates for the first-shell pairs Se- Se_1 , Se- Te_1 (Te- Se_1), and Te- Te_1 pairs. The obtained results provide insight on intrachain structure as well as on the structural and thermal disorder of mixed $\text{Se}_{1-x}\text{Te}_x$ glasses. [S0163-1829(98)05934-7]

I. INTRODUCTION

The structure of the noncrystalline $\text{Se}_{1-x}\text{Te}_x$ system has been extensively studied in amorphous (*a*, evaporated thin films), vitreous (*g*, glasses), and liquid (*l*, liquids) states using a variety of structural and spectroscopic methods: x-ray and neutron scattering,¹⁻⁶ x-ray-absorption fine-structure (XAFS) techniques,⁷⁻¹² Mössbauer spectroscopy,¹³ vibrational spectroscopy,¹⁴⁻¹⁹ and inelastic neutron scattering,²⁰⁻²² as well as by molecular-dynamics simulations.²³⁻²⁵

Under normal pressure and temperature crystalline selenium exists in five modifications. Depending on the position taken by the fifth covalent linked atom, it may exist in either helical chains (trigonal *t*-Se), Se_8 rings (α -, β -, γ -Se monoclinic forms), or Se_6 rings (rhombohedral form), which may be built if this fifth atom is placed in a *cis* or *trans* position.^{26,27} On the other hand, the crystalline tellurium exists only in the trigonal form with helical chains (*t*-Te).²⁶ Se and Te are completely miscible in each other in the liquid and solid states and form an isomorphous system (see, for example, a summary of the thermodynamics properties of $\text{Se}_{1-x}\text{Te}_x$ system).²⁸ A vitreous phase is obtained by water quenching of selenium-rich $\text{Se}_{1-x}\text{Te}_x$ liquids (below 50-at. % Te),²⁹ while by vapor deposition an amorphous (up to 50-at. % Te) or a partially microcrystalline structure (50-60-at. % Te) of $\text{Se}_{1-x}\text{Te}_x$ are produced.³⁰ It was early recognized that the local order of amorphous and liquid $\text{Se}_{1-x}\text{Te}_x$ systems are very similar in the selenium-rich range.^{4,5}

The early neutron and x-ray-scattering experiments have been described by the slightly distorted helix chain¹ or by the slightly distorted Se_8 rings² microcrystalline models. For many years amorphous Se and $\text{Se}_{1-x}\text{Te}_x$ were assumed to involve an equilibrium between chain and ring forms.^{14,15} With increasing availability of experimental data, however, it has become apparent that the ring form does not occur in an amorphous state in appreciable numbers, and the structure of *a*-Se could be viewed as infinite chains incorporating ring-like and helixlike fragments¹⁶⁻¹⁹ or as a nearly free rotating chain (NFRC).³⁻⁶ Note that the amorphous Se and the highly viscous liquid Se at the melting point are believed to consist of a chain of 10^4 – 10^6 atoms.^{31,32} Moreover, recent work indicates a variety of defect structures being present.³³⁻³⁷

Hohl and Jones²³ have given wide coverage of the structural models of pure amorphous and liquid selenium. At normal conditions the intrachain structure of *a*-Se and *l*-Se, as well as $\text{Se}_{1-x}\text{Te}_x$ mixture in the selenium-rich range, can be described by random chain models,^{3-6,16-19,33,34} with nearest-neighbor distances (Se- Se_1) intrachain (Se- Se_1 - Se_3) bond angles (θ) similar to those in the crystalline *t*-Se or α -Se, and a distribution of dihedral angles (γ) and phases. The neutron and x-ray scattering experiments have been described by the NFRC model with a completely random distribution of dihedral angles (γ).³⁻⁶ While in the other model based on x-ray photoemission spectroscopy, ultraviolet photoemission spectroscopy, and vibrational spectroscopy data,¹⁷⁻¹⁹ the dihedral angle (γ) has a fixed value (as in *t*-Se and α -Se) of about 100° , but the phase of dihedral angles in

any five-atom configuration varies in a random manner between the fixed phase of the helical chains of *t*-Se (+ + or - - helix chainlike sequence of phases) and the Se₈ ring molecule of *α*-Se (+ - or + - ringlike sequence of phases). Also, recent first-principles molecular-dynamics simulations show relatively sharp distributions of the intrachain nearest-neighbor distances (Se-Se₁) and intrachain bond angles (θ), but a wide distribution of the dihedral angle (γ) of about 100° with equilibrium between chainlike (+ + or - -) and ringlike (+ - or + -) sequences to within $\pm 5\%$.^{23,24}

Despite its overall success in the description of local order in amorphous and liquid selenium, much of information concerning two-body (pair-correlation function), three-body [intrachain Se-Se₁-Se₃ bond-angle distribution $A(\theta)$], four-body [intrachain dihedral angle distribution $D(\gamma)$], and five-body correlation functions is not directly available.²³ The situation is even more complicated, by the strong overlap of intrachain and interchain contributions in the pair-correlation functions. It is believed that the interchain (Se-Se₂) neighbor distance is substantially larger^{2,23} (3.6 Å) in the *a*-Se and *l*-Se than in the *t*-Se crystal (3.44 Å) and overlaps with the intrachain (Se-Se₃) distance (3.7 Å). During melting the density of *t*-Se decreases by about 16%, and it is suggested that the ratio of interchain to intrachain distances increases from 1.44 to 1.57.^{38,39} The choice in two configurations (helixlike and ringlike) may be remarkably correlated with the rate of the interchain and intrachain force and the composition of the Se_{1-x}Te_x.^{15,40} Moreover, the Se_{1-x}Te_x system has quite anomalous thermodynamic properties in the liquid and solid states.^{41,42,28,43} Therefore, interchain and intrachain order study by XAFS technique is particularly interesting.

Many efforts have been devoted to obtaining by the XAFS method the structural parameters of the first coordination shell of the Se_{1-x}Te_x system.⁷⁻¹⁰ Nearest-neighbor distances, coordination numbers, and Debye-Waller (DW) factors [mean-square relative displacement (MSRD) of absorber and backscatterer atoms] of Se_{1-x}Te_x glasses, thin films, and liquids have been studied.

However, relatively little is known about the distribution of intrachain (Se-Se₃) and interchain (Se-Se₂) next-nearest neighbors in pure and mixed Se_{1-x}Te_x glasses from the previous XAFS studies. The intrachain (Se-Se₃) single scattering (SS) signal has been observed at 3.69 Å in the pure *g*-Se glasses⁹ and at 3.61 Å in the isolated mixed chains in mordenite,⁹ while quantitative results have not been given for the *g*-Se_{1-x}Te_x glasses.^{9,10} On the other hand, in the crystalline *t*-Se, both next-nearest neighbors are described: the interchain Se-Se₂ at 3.37 Å and the intrachain Se-Se₃ at 3.72 Å.⁹

We suggest that an assignment of intrachain and interchain peaks may be achieved by increasing the resolution of experimental measurements and by constraining the data analysis. The XAFS measurements on the Se and Te *K* edges⁸⁻¹⁰ are generally more sensitive than the previous x-ray diffraction and neutron-scattering experiments,¹⁻⁵ because of the higher values of momentum transfer $2k$, k being the photoelectron wave vector, while the unavailability of low- k data represents a drawback in structural investigations beyond the first three shells above 4 Å.

A complete XAFS data analysis (Se and Te edges at low

and room temperature) decreases the correlation between the obtained coordination numbers and the DW factors and gives selective (Se and Te) information on local intrachain chemical ordering as well as on structural and thermal disorder. In previous XAFS studies of vitreous and amorphous Se_{1-x}Te_x only partial XAFS data analysis has been done on the first coordination shell. More complete XAFS study has been done on liquid Se_{1-x}Te_x mixtures but in a high-temperature range.¹¹

In this paper we present a complete XAFS study of the first shell of Se_{1-x}Te_x glasses: nearest-neighbor distances, coordination numbers (intrachain chemical ordering), DW factors [structural and thermal disorder on both the Se and Te *K* edges at low (80 K) and room temperatures].

In a future paper will be presented a complete XAFS study of second shells (intrachain and interchain) of *g*-Se at low (26 and 80 K) and room temperatures and a partial (only Se *K*-edge data) XAFS study of second shells (intrachain and interchain) of Se_{1-x}Te_x glasses at low temperature (80 K).

The obtained local environment built on random chain model is compared with the existing structural models.

A detailed XAFS analysis of experimental data is carried out by extended XAFS data analysis (EDA) software code.⁴⁴⁻⁴⁶ As it was shown recently by Ma *et al.*⁴⁷ and McKale *et al.*,⁴⁸ phase shifts of heavy atoms like Te give shorter distances than their crystallographic ones and large threshold energy shifts. In the previous articles on Se_{1-x}Te_x mixtures^{9,10} the XAFS results have been analyzed using McKale *et al.*'s phase shifts and amplitudes. Therefore, we have used improved multiple-scattering FEFF6 code⁴⁹ for the phase shifts and amplitude calculations.

A preliminary report has been presented elsewhere.⁵⁰

The paper is organized as follows: in Sec. II, the experimental procedure of XAFS measurements at the Se and Te *K* edges in Se_{1-x}Te_x is described; in Sec. III, we present data treatment procedures, discuss the origin of several contributions to XAFS, and present the results; in Sec. IV, we compare our results with the ones from XAFS and other experimental techniques; in Sec. V, the summary of present work and main conclusions are given.

II. EXPERIMENT

The Se_{1-x}Te_x mixtures were prepared by weighing the elements Se and Te, in convenient proportions for x values ranging from 0 to 0.4. We used pure selenium (Koch-light, 5 N) and pure tellurium (Fluka, 5 N). In order to prevent oxidation, glasses were formed by direct fusion of the pure elements in a silica tube sealed under vacuum ($\approx 10^{-1}$ Pa). The temperature is slowly raised up to 323 K above the melting point and is kept at this temperature, typically for 24 h. Then the melt is quenched into cold water. All the samples have been checked to be amorphous by x-ray diffraction and differential scanning calorimetry (Perkin-Elmer DSC7).

The samples for XAFS measurements were finely ground and the powder was sandwiched between many layers of Scotch tape. The influence of the sample thickness was controlled at different compositions.

X-ray absorption spectra at the Se *K* edge were measured in transmission using a standard setup of the DCI D21 (XAFS-2) beam line at LURE (Orsay): ring current, 350-

250 mA; beam energy, 1.85 GeV. The experimental spectra at three different temperatures (26 K, 80 K, and room temperature) were measured by two ionization chambers filled with argon. The measurements were done from 12 500 to 13 500 eV ($E_0 = 12\,658$ eV) with the step 2 eV, count rate 2 s per point, and the energy resolution [half width at half maximum (HWHM)] being 2.5 eV [Si(311)]. A 50% rejection of harmonic was achieved by slightly detuning the two crystals from the parallel alignment. The edge position were reproducible to better than 0.2 eV.

The Te K -edge XAFS spectra at low (80 K) and room temperatures were measured in transmission mode at the NSLS storage ring using the X11A station (BNL, Upton). The electron energy was 2.5 GeV with current about 175 mA. The synchrotron radiation was monochromatized using the Si(311) two-crystal monochromator, and its intensity was measured by two ionization chambers containing argon gas. The spectra were measured in the energy range 31 400–32 500 eV ($E_0 = 31\,813$ eV) with an energy step 5 eV, count rate 2 s per point, and an energy resolution (HWHM) equal to about ~ 6 eV. In the case of Te, the edge position alignment was obtained at the first inflection point. Ten independent measurements were averaged to obtain a better signal-to-noise ratio.

The crystalline t -Se and t -Te with the trigonal structure were used as reference compounds. Their XAFS was recorded under the same conditions as for glasses. Moreover, the additional measurements of reference t -Te were done on the Te K edge in transmission mode at the DORIS III storage ring (HASYLAB, Hamburg) using the Römo II XAFS station on the X1.1 wiggler beamline. A report on crystalline t -Te has been presented elsewhere.⁵¹ We have obtained excellent agreement between two sets of measurements and known crystallographic data.²⁶

III. DATA ANALYSIS AND RESULTS

The experimental data were analyzed by the XAFS data analysis software package EDA implementing the standard data analysis procedure with improved algorithms.⁴⁴ Previously the analysis procedure was verified by Kuzmin and Purans on disordered crystalline and amorphous systems.^{45,46} A brief description of the analysis procedure is given below.

The background contribution $\mu_b(E)$ was approximated by a polynomial $\mu_b = A + B/E^3$ and subtracted from the experimental spectrum $\mu(E)$. Further, the atomiclike contribution $\mu_0(E)$ was calculated by a combined polynomial/cubic-spline technique in order to have a precise removal of the XAFS signal zero line, and finally the XAFS signal $\chi(E)$ was determined as $\chi(E) = (\mu - \mu_b - \mu_0)/\mu_0$. We convert $\chi(E)$ to a space of the photoelectron wave vector k , defined as $k = \sqrt{(2m/\hbar^2)(E - E_0)}$, where $(E - E_0)$ is the photoelectron kinetic energy. The experimental XAFS signal $\chi(k)$ was multiplied by a factor k^2 to compensate the decrease of its amplitude with the increase of the wave vector value (see curves in Fig. 1 and Fig. 2).

The Fourier transforms (FT) of the experimental XAFS signal, with a Kaiser-Bessel window⁴⁴ ($A = 1.5$) in the range from 1.0 to 16 \AA^{-1} (Se) and from 1.0 to 14 \AA^{-1} (Te) are shown in Figs. 3–5. For pure selenium (t -Se and g -Se) the evolution of FT with the temperature (26 K, 80 K, and RT)

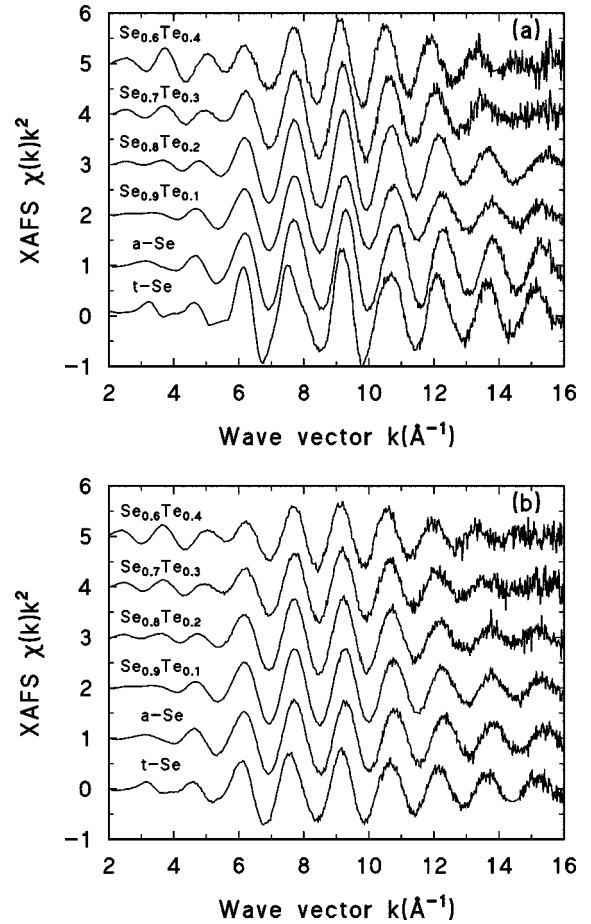


FIG. 1. Experimental XAFS $\chi(k)k^2$ spectra of the $\text{Se}_{1-x}\text{Te}_x$ glasses at the Se K edge: low temperature (80 K) (a) and room temperature (b). All spectra are plotted on the same vertical scale and displaced vertically for clarity.

are presented in Fig. 3. The first peak in the FT is sharp for crystalline and vitreous states at all temperatures. When temperature is raised the amplitude of the first-shell peak decreases due to increase of the thermal disorder. For crystalline t -Se the amplitude of the next shell peaks declines more rapidly, while for vitreous g -Se its amplitude is much less than in crystalline t -Se, but decreases slowly. As one can see (Figs. 4 and 5) the magnitude of the first peak at both the Se and Te K edges decreases and its position also shifts to higher distances as Te content increases. Notice that all FT presented in this paper are not corrected for the photoelectron phase shift; therefore, the positions of peaks differ from the true values.

The previous neutron and x-ray scattering studies on the $\text{Se}_{1-x}\text{Te}_x$ glasses have shown that the first minimum of the radial distribution function (RDF) above the first coordination shell is near zero;^{1–5} therefore, the contributions of first coordination shell (Se and Te) are well separated from the next shell's contributions in the glasses. The contributions of first-shell atoms to the total XAFS signal were singled out by back FT in the range 1.0–2.7 \AA for Se surrounding and 1.5–3.0 \AA for Te surrounding (see first well visible peak in Figs. 3–5). The XAFS $\chi(k)k^2$ signal ($k = 4.5$ –16.0 \AA^{-1} Se and $k = 5.0$ –14.0 \AA^{-1} Te) thus obtained was utilized in the best-fit multishell analysis procedure.

The fitting procedure of the XAFS spectra was based on

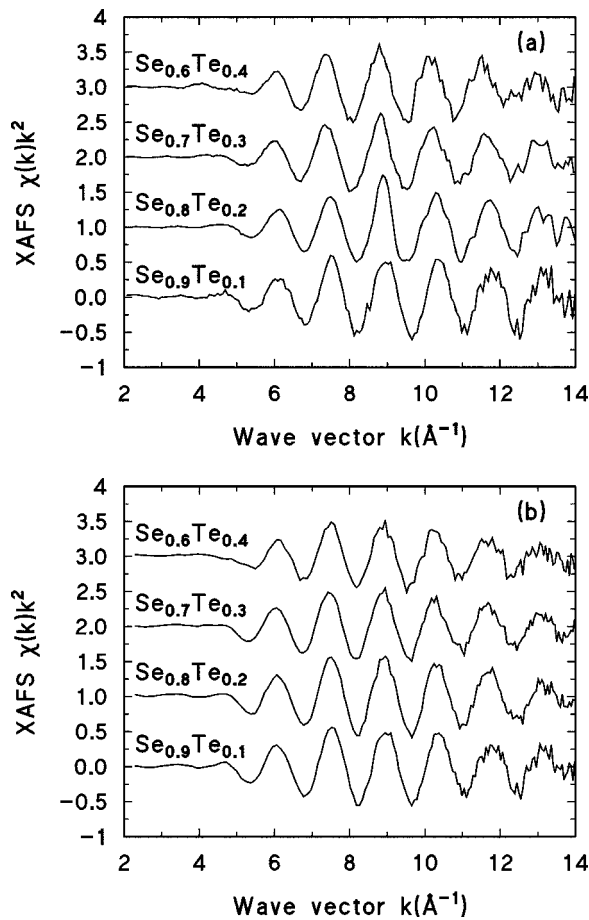


FIG. 2. Experimental XAFS $\chi(k)k^2$ spectra of the $\text{Se}_{1-x}\text{Te}_x$ glasses at the Te K edge: low temperature (80 K) (a) and room temperature (b). All spectra are plotted on the same vertical scale and displaced vertically for clarity.

the single-scattering curved-wave formalism.⁵²⁻⁵⁵ The XAFS $\chi(k)$ was calculated using the expression

$$\chi(k) = \sum_i \frac{N_i}{kR_i^2} f_i(\pi, k, R_i) e^{-2\sigma_i^2 k^2} \sin[2kR_i + \phi_i(\pi, k, R_i)], \quad (1)$$

where N_i is the coordination number of the i shell, R_i is the radius of the i shell, σ_i is the Debye-Waller factor, $f_i(\pi, k, R_i)$ is the backscattering amplitude of the photoelectron by atoms of the i -coordination shell, and $\phi_i(\pi, k, R_i)$ is the phase shift of the photoelectron determined by central and scattering atoms. Equation (1) is only valid when the radial distribution of each shell may be approximated by a Gaussian. This restriction can be removed and Eq. (1) modified to include asymmetric distribution.^{56,57} See, for example, the XAFS analysis of amorphous and crystalline Ge.⁵⁸⁻⁶¹ For the results described in this work (particularly the first coordination shell) the simple form of Eq. (1) is adequate, and the corrections of the distances are small.

Backscattering amplitudes $f(\pi, k, R)$ and phases $\phi(\pi, k, R)$ were calculated by the FEFF6 code⁴⁹ for clusters of four coordination shells with the crystallographic data from t -Se, t -Te (Ref. 26) and model (chemical ordered) t - $\text{Se}_{0.5}\text{Te}_{0.5}$ compound: Se- Se_1 pair ($R=2.37$ Å), Se- Te_1 pair ($R=2.54$ Å), and Te- Te_1 pair ($R=2.83$ Å). The first-

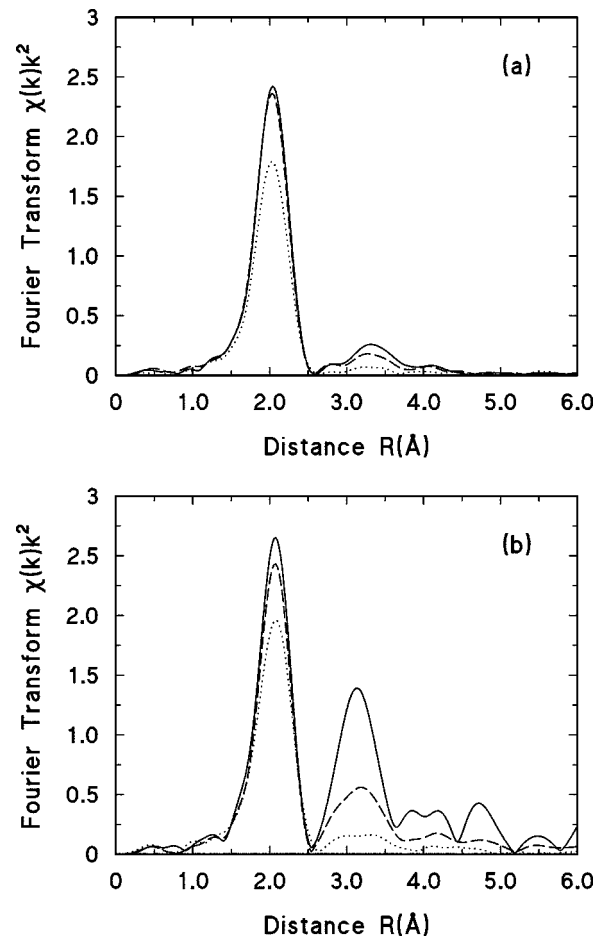


FIG. 3. FT modulus of the experimental XAFS $\chi(k)k^2$ (Se K edge) at the different temperatures: at 26 K (solid line); 80 K (long dashed line); room temperature (dotted line). (a) a -Se and (b) t -Se.

shell single scattering contributions are presented on Fig. 6 for the model t - $\text{Se}_{0.5}\text{Te}_{0.5}$ compound: Se(Te)- Se_1 (DW factor 0.02 Å²), Se- Te_1 (DW factor 0.02 Å²), and Te- Te_1 (DW factor 0.03 Å²).

The photoelectron mean-free-path contribution was automatically included in the scattering-amplitude function by the use of the complex Hedin-Lundqvist exchange and cor-

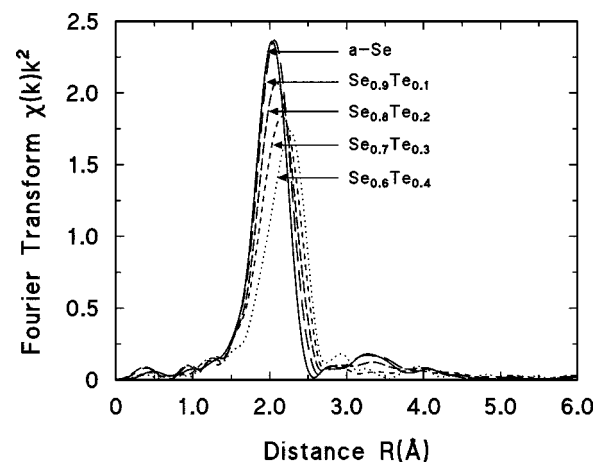


FIG. 4. FT modulus of the experimental XAFS $\chi(k)k^2$ of $\text{Se}_{1-x}\text{Te}_x$ glasses at the Se K edge at (80 K).

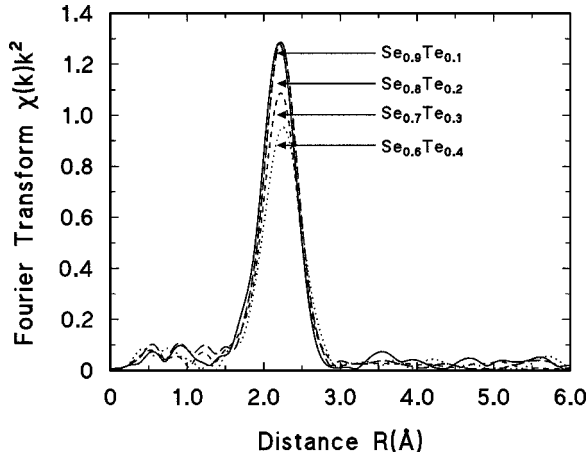


FIG. 5. FT modulus of the experimental XAFS $\chi(k)k^2$ of $\text{Se}_{1-x}\text{Te}_x$ glasses at the Te K edge at (80 K).

relation potential in the scattering-amplitude calculation.⁴⁹ Natural broadening was included through the core-level width $\Gamma_{\text{core-hole}} = 2.8$ eV (Se) and 11 eV (Te).⁴⁹

The maximum number of fitting parameters is limited in general case by the number of independent data points $N_{\text{ind}} \approx 2\Delta k\Delta R/\pi + 2$, where Δk and ΔR are, respectively, the

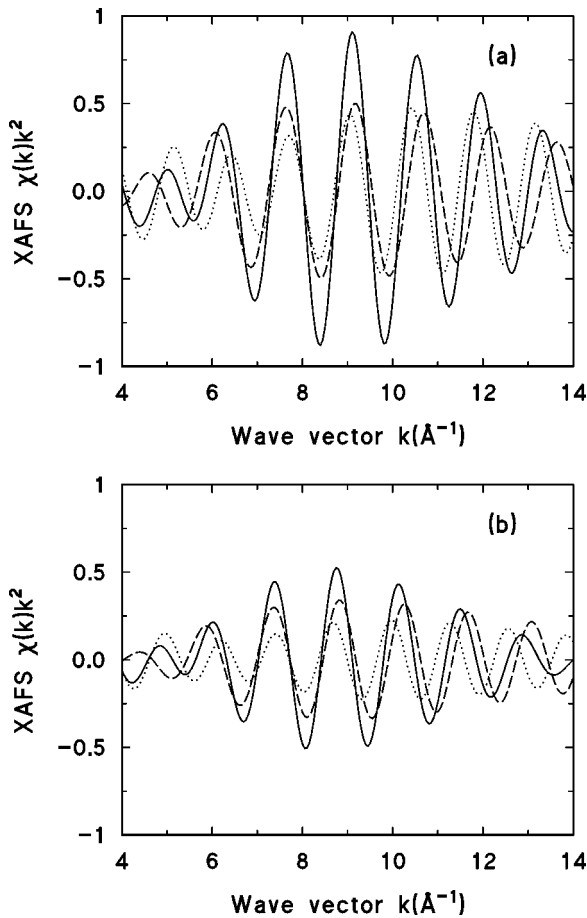


FIG. 6. Single-scattering XAFS contributions at the Se (a) and Te (b) K edges calculated for the model $t\text{-Se}_{0.5}\text{Te}_{0.5}$ compound and broadened with a DW factor of 0.002 \AA^2 : Se(Te)- Se_1 (dashed line), Se(Te)- Se_1 (dotted line), Te- Te_1 (dotted line), total signal (full line).

widths in k and R space used in the fit.⁶² In the case of the first coordination shell of Se, N_{ind} is equal to 13.7 ($\Delta k = 11.5$ and $\Delta R = 1.6$), and in the case of Te, N_{ind} is equal to 10.6 ($\Delta k = 9$ and $\Delta R = 1.5$).

The total coordination number at the Se K edge is restricted, which is assumed to be two ($N_1 + N_2 = 2$). Therefore, we used two shell models (Se- Se_1 and Se- Te_1) with five varying parameters and the fitting parameters were distances, DW factors, and the ratio between the coordination numbers. In comparison, we fitted the data also with the single-shell models (Se- Se_1) with three varying parameters and the fitting parameters were distance, DW factor, and the coordination number.

The coordination numbers between the two edges are constrained. Note, that the experimental data at the Te K edge are lower quality than the good quality data at the Se K edge. Therefore, the coordination numbers (Te- Se_1 and Te- Te_1) are calculated using the obtained coordination numbers at the Se K edge for the same glasses: $N_3 = N_2x/(1-x)$ and $N_4 + N_3 = 2$. At the Te K edge, we used two shell models (Te- Se_1 and Te- Te_1) with four varying parameters and the fitting parameters were distance and the DW factor. In comparison, we used also the single-shell models (Te- Se_1) with two varying parameters and the fitting parameters were distance and the DW factor.

The results of the fitting procedure for the first shell are presented in Table I. The fitting error ε is calculated by Eq. (2) of Ref. 46.

Note that the obtained crystallographic parameters for $t\text{-Se}$ and $t\text{-Te}$ are in good agreement with the x-ray-diffraction data.²⁶ In the case of the K edge of Se and Te, E_0 is located near the first inflection point. Appropriated values for E_0 and S_0^2 were calibrated by fitting the low-temperature (LT) first-shell spectra of the reference $t\text{-Se}$ and $t\text{-Te}$ (the overall amplitude reduction factor S_0^2 was obtained at about $S_0^2 = 1$).

Based on the fitting parameters, the RDF can be reconstructed according to the equation of the sum of Gaussian distributions,

$$4\pi\rho r^2g(r) = \sum_i (N_i/\sqrt{2\pi\sigma_i^2})\exp[-(r-R_i)^2/(2\sigma_i^2)], \quad (2)$$

in which $g(r)$ is the pair-correlation function, and ρ is the atomic-number density. We used the data for vitreous selenium to calculate $g(r)$.³⁹ This graphical representation (see Figs. 7 and 8) is useful since it takes into account not only coordination numbers and peak positions but also DW factor values and overlap of different shell contributions.

The composition evolution of the probability that Se and Te atoms are distributed around a central Se atom is presented in Fig. 9. We have compared the results with a model of chemical order and chemical disorder inside the chain. The composition variation of Se- Se_1 and Se- Te_1 bond lengths is presented in Figs. 10 and 11 at room and low temperatures in comparison with the Inui *et al.*⁹ work for mixture glasses at 80 K and the work of Inui and co-workers¹¹ for liquid mixture, as well as the work of Yang *et al.*¹⁰ for amorphous thin films (80 K). The temperature

TABLE I. Structural data obtained from the best-fit analysis of the Se and Te K edges XAFS in $\text{Se}_x\text{Te}_{1-x}$ [N is the number of Se (± 0.1) or Te (± 0.1) atoms located in the first shell of Se or Te at a distance R from the Se (± 0.005 Å) or Te (± 0.007 Å)]; σ^2 is the DW factor (± 10 %, while $\pm 20\%$ on Te-Te₁); ε is the fitting error calculated by Eq. (2) of Ref. 46.

Compound	Se K edge		Se-Te ₁			Se-Te ₁		ε ($\times 10^{-4}$)
	LT (80 K)	N_1	R_1 (Å)	σ_1^2 (Å ²)	N_2	R_2 (Å)	σ_2^2 (Å ²)	
t -Se (26 K)		2.00	2.371	0.0017				3.0
t -Se		2.03	2.370	0.0021				3.6
a -Se (26 K)		1.96	2.341	0.0018				5.2
a -Se		1.94	2.340	0.0020				5.4
a -Se _{0.9} Te _{0.1}		1.75	2.344	0.0020	0.25	2.539	0.0021	3.4
a -Se _{0.8} Te _{0.2}		1.50	2.345	0.0021	0.50	2.540	0.0021	2.6
a -Se _{0.7} Te _{0.3}		1.20	2.347	0.0022	0.80	2.543	0.0021	4.1
a -Se _{0.6} Te _{0.4}		0.88	2.363	0.0026	1.12	2.557	0.0025	5.5
	Se K edge		Se-Te ₁			Se-Te ₁		ε ($\times 10^{-4}$)
	RT	N_3	R_3	σ_3^2	N_4	R_4	σ_4^2	
t -Se		1.99	2.365	0.0037				5.6
a -Se		1.96	2.341	0.0036				5.1
a -Se _{0.90} Te _{0.1}		1.76	2.342	0.0035	0.24	2.541	0.0038	2.9
a -Se _{0.8} Te _{0.2}		1.54	2.347	0.0036	0.46	2.543	0.0040	4.4
a -Se _{0.7} Te _{0.3}		1.20	2.348	0.0036	0.80	2.543	0.0042	3.7
a -Se _{0.6} Te _{0.4}		0.95	2.360	0.0040	1.05	2.551	0.0042	3.6
	Te K edge		Te-Te ₁			Te-Te ₁		ε ($\times 10^{-4}$)
	LT (80 K)	N_3	R_3	σ_3^2	N_4	R_4	σ_4^2	
a -Se _{0.9} Te _{0.1}		2.00	2.538	0.0023				3.0
a -Se _{0.8} Te _{0.2}		2.00	2.544	0.0022				1.0
a -Se _{0.7} Te _{0.3}		1.90	2.546	0.0023	0.10	2.743	0.0017	1.0
a -Se _{0.6} Te _{0.4}		1.65	2.548	0.0027	0.35	2.745	0.0017	2.0
t -Te					1.97	2.840	0.0017	12
	Te K edge		Te-Te ₁			Te-Te ₁		ε ($\times 10^{-4}$)
	RT	N_3	R_3	σ_3^2	N_4	R_4	σ_4^2	
a -Se _{0.9} Te _{0.1}		2.0	2.540	0.0038				8.7
a -Se _{0.8} Te _{0.2}		2.0	2.544	0.0040				2.9
a -Se _{0.7} Te _{0.3}		1.9	2.545	0.0040	0.1	2.740	0.0040	1.5
a -Se _{0.6} Te _{0.4}		1.65	2.555	0.0040	0.35	2.747	0.0040	2.5
t -Te					2.0	2.827	0.0059	2.8

dependencies of first-shell DW factors of Se-Se₁, Se-Te₁, and Te-Te₁ bonds are shown in Fig. 12.

Statistic evaluation of the results. Recently, the statistical evaluation of XAFS results and the reliability of the theoretical standards (phases and amplitudes generated by FEFF5 code) have been reviewed for the SS one-shell analysis.⁶³ In general, good agreement with crystallographic data is achieved, with typical errors of order 0.005 Å for nearest-neighbor distances R and of order 5% for the DW factors. The observation was also done to evaluate the correlation errors between the parameters. Two sets of variables are strongly correlated: coordination number and DW factor and distance and E_o .

In this paper to decrease the correlation between these parameters the total coordination number and E_o are constrained (see above). On the other hand, the correlation be-

tween two shell parameters can lead to additional uncertainties for the extracted XAFS parameters. Therefore, the set of the two-shell fit is done at the Se K edge on the experimental spectra (LT and RT) of glasses with different composition. In Fig. 13, the fitting errors are plotted for various values of first-shell (Se-Se₁) coordination numbers N_1 with constrained values of second-shell (Se-Te₁) coordination numbers N_2 , while the DW factors are free.

To examine the significance of adding a second shell to the XAFS analysis, the method based on F test is used.⁶⁴ The adding of the second shell in the fit is significant on the Se K edge for all measured mixed glasses, while on the Te K edge it is only significant above 20-at. % Te. Note, that for the two-shell fit the total coordination number was constrained to two. Therefore, the results of two-shell fit are presented on the Se K edge for all mixed glasses and on the Te K edge at

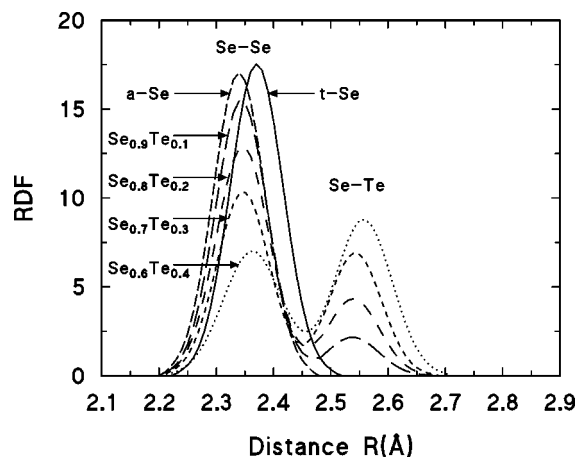


FIG. 7. Reconstructed RDF's of the first coordination shell of $\text{Se}_{1-x}\text{Te}_x$ glasses around Se at low temperature (80 K).

30- and 40-at. % Te, while at 30- and 40-at. % Te only the results of the one-shell fit are shown.

IV. DISCUSSION

In the following, we will compare the existing structural results of $\text{Se}_{1-x}\text{Te}_x$ glasses and liquid and disordered crystals with our XAFS results with regard to structural parameters and reconstructed Se and Te local environment. Note that XAFS measurements of $\text{Se}_{1-x}\text{Te}_x$ glasses carried out on both the Se and Te K edges at low and room temperatures significantly improve the reliability of obtained structural parameters (Tables I).

Intrachain chemical ordering. As was previously suggested from x-ray-diffraction and Mössbauer studies, the Se-Te bond in the solid state is stronger than the average of the Se-Se and Te-Te bonds^{39,65} that is generally ascribed to a certain amount of ionic character in the Se-Te bond.^{65,66} The previous neutron-scattering experiments done by Bellissent and Tourand^{4,5} on amorphous $\text{Se}_{1-x}\text{Te}_x$ were described by the NFRC model with a completely random distribution of Se and Te atoms in the chains and with the randomness of the dihedral angle. Unfortunately, the lack of suitable isotopes to separate out the partial (Se and Te) RDF's has sig-

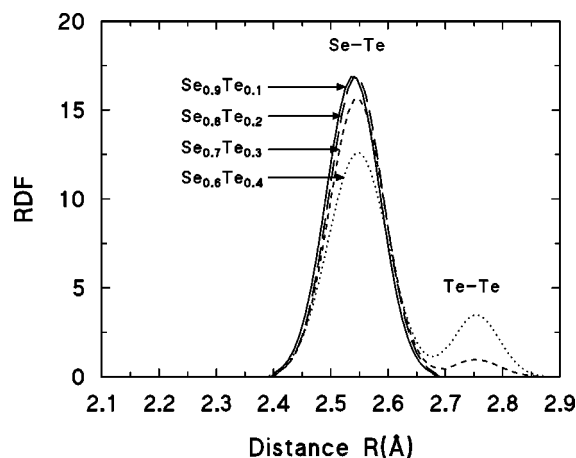


FIG. 8. Reconstructed RDF's of the first coordination shell of $\text{Se}_{1-x}\text{Te}_x$ glasses around Te at low temperature (80 K).

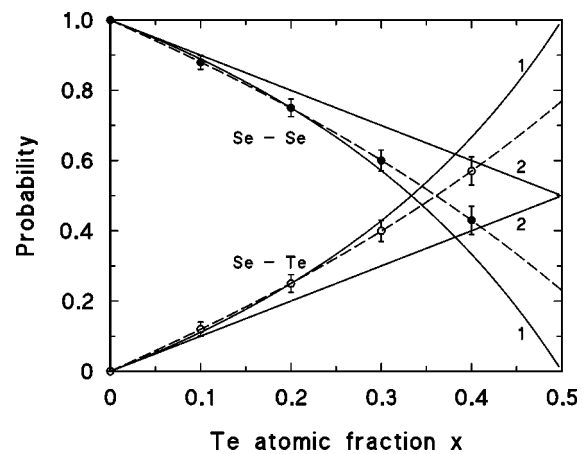


FIG. 9. The composition evolution of the probability that Se and Te atoms are distributed around a central Se atom. Probabilities are the values calculated from the data at the low temperature of Table I. Curves 1 are calculated for full chemical order, while curves 2 for full chemical disorder. The dashed lines are guides for the eye.

nificantly limited the quantitative structural information yielded by the previous neutron-scattering studies.^{4,5,47} Also the previous XAFS results have suggested completely random distribution of atoms, at least at the Se sites.^{9,10} While recently Ohmasa *et al.*⁶⁷ and Ikawa⁶⁸ claimed that the distribution of Se and Te in the lattice has not been clarified yet, experimentally. It does not seem completely random or regular.

The present first shell XAFS data (see Table I) show the evolution of the intrachain *chemical ordering*. The composition dependencies are calculated and presented in Fig. 9. Curves 1 are calculated for the full chemical disorder, while curves 2 for the full chemical order. On the curves 1 and 2 are presented the normalized coordination numbers ($N_i/2$) of Se- Se_1 and Se- Te_1 pairs, respectively. We found that the number of Se- Te_1 , Te- Se_1 , and Te- Te_1 bonds increases, but the number of Se- Se_1 bonds decreases more rapidly with Te content in the glasses than would be suggested by the model

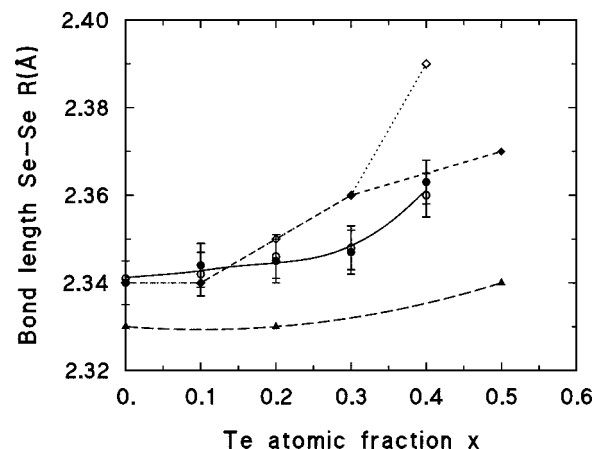


FIG. 10. The composition variation of Se-Se bond length: this work, glasses at low (full circle) and room (open circle) temperatures; Inui *et al.* (Ref. 9) work, glasses at 80 K (open diamond); Tamura *et al.* (Ref. 11) work, liquid mixture (full triangle); Yang *et al.* (Ref. 10) work, amorphous thin films at 80 K (full diamond). The solid, dashed, and dotted lines are guides for the eye.

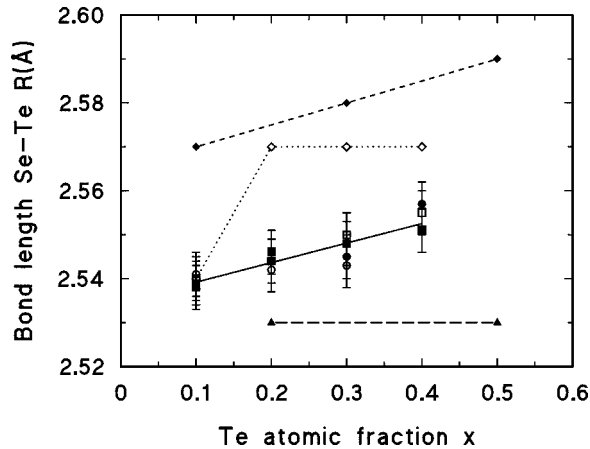


FIG. 11. The composition variation of Se-Te bond length: this work, glasses at the Se K edge at low (full circle) and room (open circle) temperatures; this work, glasses at the Te K edge at low (full square) and room (open square) temperatures; Inui *et al.* (Ref. 9) work, glasses at 80 K (open diamond); Tamura *et al.* (Ref. 11) work, liquid mixture (full triangle); Yang *et al.* (Ref. 10) work, amorphous thin films at 80 K (full diamond). The solid, dashed, and dotted lines are guides for the eye.

of a completely random distribution of Se and Te atoms in the chains. Therefore, we suggest that the distribution of the Se- Te_1 (Te- Se_1) bonds shows a predominant contribution.

These results on the Se K edge are in a partial agreement, but on the Te K edge they show discrepancies with the previous XAFS study.^{9,10} Yang *et al.*¹⁰ suggest the random distribution at the Se sites and unrandom distribution (alternating manner) at the Te sites (coordination number corresponding to one Te- Te_1 and one Te- Se_1 pair does not change with composition of the amorphous thin films). Unfortunately, the DW factors values are absent in their paper. On the other hand, Inui *et al.*⁹ have done measurements of glasses on the Se K edge and suggest that Se and Te atoms in the chain are randomly distributed at both sites. But also in

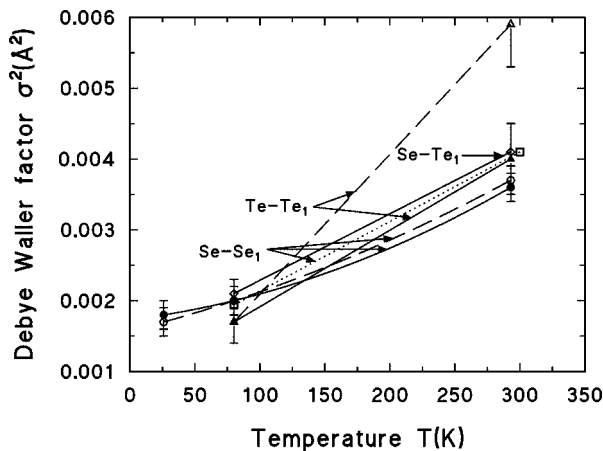


FIG. 12. The temperature dependence of DW factors: this work, Se- Se_1 pairs in g -Se (full circle and full line) and in t -Se (open circle and dashed line); this work, Se- Te_1 pairs in g - $\text{Se}_{1-x}\text{Te}_x$ (open diamond and full line); this work, Te- Te_1 pairs in g - $\text{Se}_{1-x}\text{Te}_x$ (full triangle and full line) and in t -Te (open triangle and dashed line); Tamura *et al.* (Ref. 11) work, Se- Se_1 in t -Se (open square and dotted line).

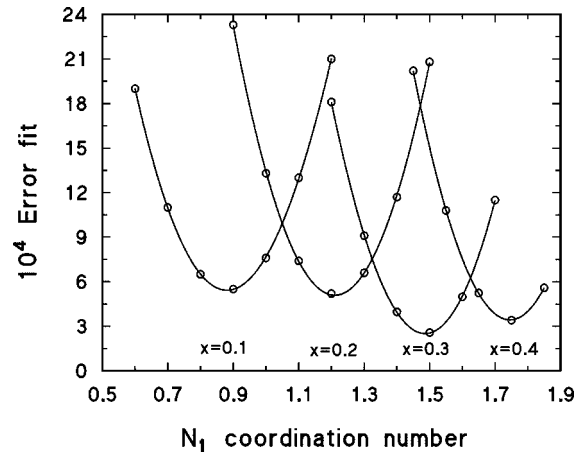


FIG. 13. A plot of two-shells fitting errors for various values of first-shell (Se- Se_1) coordination numbers N_1 with constrained values of second-shell (Se- Te_1) coordination numbers N_2 and free DW factors. The fittings were done at the Se K edge on the experimental spectra (LT) of the $\text{Se}_x\text{Te}_{1-x}$ glasses with different composition.

their work we can see remarkable deviation of the coordination number ratio from completely random distribution of atoms (see Fig. 10 in Ref. 9). The obtained wide spread of the DW factors (see Table II in Ref. 9) that significantly influences the values of coordination numbers reduces the probability of their conclusion.

Intrachain bond distances. First, we confirm the previous results⁷⁻¹⁰ (see Fig. 10) that for the pure Se the distance Se- Se_1 along the chain reduces from 2.37 Å in t -Se crystal to about 2.34 Å in g -Se glass, which is in good agreement with the x-ray [2.33 Å (Ref. 1) and 2.34 Å (Ref. 2)] and neutron [2.33 Å (Ref. 1) and 2.32 Å (Ref. 5)] scattering experimental data.

Second, the comparison presented in Figs. 10 and 11 of the previous [Table I (Ref. 10) and Table II (Ref. 9)] and present (see Table I) experimental XAFS results shows an elongation of the Se- Se_1 and Se- Te_1 distances with the addition of Te. The Se K -edge XAFS study (80 K) of g - $\text{Se}_{1-x}\text{Te}_x$ glasses and isolated Se-Te mixed chains confined in the mordenite channels^{8,9} has shown that the Se- Se_1 bond of the isolated mixed chains in mordenite elongates gradually (2.33–2.37 Å) with the addition of Te, while the Se- Te_1 bond changes little. The distances in the g - $\text{Se}_{1-x}\text{Te}_x$ glasses change in the ranges Se- Se_1 (2.34–2.39 Å) and Se- Te_1 (2.54–2.57 Å), but XAFS data on the Te K edge were not available before. The XAFS study (80 K) of amorphous $\text{Se}_{1-x}\text{Te}_x$ thin films has been developed on both the Se and Te K edges¹⁰ and it has shown three bond types: Se- Se_1 (2.34–2.37 Å), Se- Te_1 (2.57–2.59 Å), and Te- Te_1 bonds (2.72 Å). The authors suggest that an introduction of more Te leads to longer bonds of Se- Se_1 and Se- Te_1 , while the Te- Te_1 (short-type) bond lengthens slightly with increasing Te content. But as can see from Table 6 of Ref. 11 these changes are very small in the selenium-rich range of $\text{Se}_{1-x}\text{Te}_x$ mixtures: Se- Se_1 (2.33–2.34 Å), Se- Te_1 (2.53 Å), and Te- Te_1 (2.75 Å). The authors suggest two types of

Te-Te₁ bonds: a short one at 2.74–2.76 Å and long one at 2.92–2.97 Å.

The present analysis of the distances (see Figs. 10 and 11) shows a small elongation with Te content with the composition Se_{0.7}Te_{0.3}: (i) Se-Se₁ from 2.340 Å to 2.347 Å, that is in agreement with the previous results; (ii) Se-Te₁ (Te-Se₁) from 2.540 Å to 2.545 Å, that is in partial agreement with the previous results; and (iii) Te-Te₁ from 2.725 Å to 2.740 Å. As for us, we observed that the distances in glasses suddenly increase with the composition Se_{0.6}Te_{0.4} up to 2.360 Å (Se-Se₁), 2.550 Å (Se-Te₁, Te-Se₁) and 2.745 Å (Te-Te₁). Probably these results are related to a more ordered structure in the glasses near the stoichiometric composition. As can be seen from Fig. 10, a general agreement is obtained between the all measurements of Se-Se₁ distances in noncrystalline solids. With the addition of Te is observed the increasing discrepancy that may imply the sensitivity of structure to the preparation conditions near the crystallization boundary and near the stoichiometric composition. On the other hand, only partial agreement is obtained with the previous results concerning the Se-Te₁ distances.

t-Se and *t*-Te crystals are good reference compounds for the Se-Se₁ and Te-Te₁ pairs, respectively, while for Se-Te₁ and Te-Se₁ pairs a good reference compound is absent (AsI₃ is not a good reference compound for the Te-Se₁ pair); that explains why the observed discrepancy is greater for the Se-Te₁ pair than for the Se-Se₁ pair. Moreover, in the previous articles an Se_{1-x}Te_x mixtures the XAFS results have been analyzed using McKale *et al.*⁴⁸ or empirical¹⁰ phase shifts and amplitudes. Therefore, we have used the improved multiple-scattering FEFF6 code⁴⁹ for the phase shifts and amplitude calculations. The present experimental data have additional experimental evidence: the independent measurements on both the Se and Te *K* edges at low and room temperatures coincide completely (see Table I) in the error bar of the measurements that significantly improve the reliability of obtained structural parameters.

The recent XAFS study of a liquid *l*-Se_{1-x}Te_x mixtures¹¹ has shown the same, as in present study, increase of Se-Se₁ and Se-Te₁ distances in the selenium-rich range. We suggest that the observed difference (see Figs. 10 and 11) is due to the different temperature of measurements (glasses at 80 K and liquids at 673–773 K) and probably also due to a cumulant correction that must be included at high temperature with greater DW factors. See, for example, the cumulant analysis of the XAFS data of amorphous and crystalline Ge done by Dalba and co-workers^{58,59}

The first question concerns why for the first coordination shell of Se and Te the distances along the chain reduce from 2.37 Å (Se-Se₁) and 2.83 Å (Te-Te₁) in trigonal crystals *t*-Se and *t*-Te to about 2.34 Å (Se-Se₁) and 2.73 Å (Te-Te₁) in glasses and amorphous thin films.^{7–10} For Se-Te₁ pairs the distance along the chain also reduces from 2.61 Å in the mixed crystals to about 2.54 Å in glasses and amorphous thin films.^{7–10} Note that the difference of distances in the crystalline and amorphous states progressively increases from 0.03 Å (Se-Se₁) to 0.07 Å (Se-Te₁) and up to 0.1 Å (Te-Te₁). Therefore, the intrachain bonds are stronger for the amorphous state than for the trigonal crystalline state, as is also manifested by vibrational spectroscopy for *a*-Se.^{14,15,69} Usu-

ally it was suggested from the study of isolated Se_{1-x}Te_x chains in mordenite channels that the covalent intrachain bonds become stronger and shorter when the interchain interaction is reduced.^{8,9} Also, for amorphous Se it is suggested that the interchain interaction is weaker than in *t*-Se.^{8,9}

The second question concerns why the intrachain distances elongate as Te content increases. Semiempirical model studies of electronic and lattice structures of Se_{1-x}Te_x chains have explained the observed increase of the bond lengths as Te content increases.⁷⁰ By replacing Se with Te atoms in the chain the charge transfer occurs in a larger extent from Te so that the lengths of the bonds receiving the charge transfer become longer. On the other hand, there is another more popular explanation possible.^{9,71} It is known from x-ray-diffraction measurements that the ratio of the nearest interchain distance to the intrachain covalent bonds length is 1.21 for *t*-Te and 1.45 for *t*-Se.²⁶ This suggests that the interchain bonding is stronger in *t*-Te than in *t*-Se. When Se atoms are substituted by Te atoms, the interchain bonding is expected to strengthen, which results in a decrease of the interchain bond strength.^{9,71} In spite of the lack of the interchain interaction in single helical chains in linear mordenite channels, the bond lengths (Se-Se₁ and Se-Te₁), as well as the Mössbauer parameters, vary similar to those in the Se_{1-x}Te_x glasses; therefore, the authors have suggested an additional intrachain interaction with a charge transfer governs the process.⁷¹

Intrachain thermal and structural disorder. The first-shell DW factors of Se-Se₁ and Se-Te₁ (Te-Se₁) bonds show a similar temperature behavior, while Te-Te₁ bonds show a slightly different behavior (see Table I and Fig. 12). In the error bar of measurements the DW factors are independent of the glasses composition. As is usual for amorphous systems,⁵⁹ we supposed that the difference between DW factors in amorphous and crystalline states at low temperature gives the structural contribution to the width of the distribution, while a temperature dependence gives the thermal contribution in Se_{1-x}Te_x glasses. Moreover, the temperature dependence of the DW factors gives a measure of the effective bond-stretching force constant between absorber and back-scatterer atoms.^{58,59} Obviously, to compare the thermal disorder of vitreous and crystalline states we must take into account that these intrachain bonds are a little stronger in glasses than in the reference trigonal crystals [see the Se-Se₁, Se-Te₁, and Te-Te₁ distances in Table I and the stretching modes for Se-Se₁ (Refs. 14,15 and 20–22)]. Therefore, we suppose a small decrease of thermal contribution to the total DW factor for the Se-Se₁ bond and a greater decrease for Se-Te₁, and Te-Te₁ bonds in accordance with the reduction of the distances in the amorphous state.

First, the DW factors of Se-Se₁, and Se-Te₁ (Te-Se₁) at low (80 K) temperature are about 0.0020–0.0026 Å² and increase with the temperature up to a 0.0035–0.0042 Å² value for the glasses and for the crystals (see Table I). Therefore, we suggest that thermal disorder gives the main contribution to the DW factors of Se-Se₁, and Se-Te₁ (Te-Se₁) pairs at room as well as at low temperatures.

Second, the DW factors of the Te-Te₁ bonds at low temperature are about 0.0017 Å² for the glasses as well as for the crystalline *t*-Te and the factors increase with the tempera-

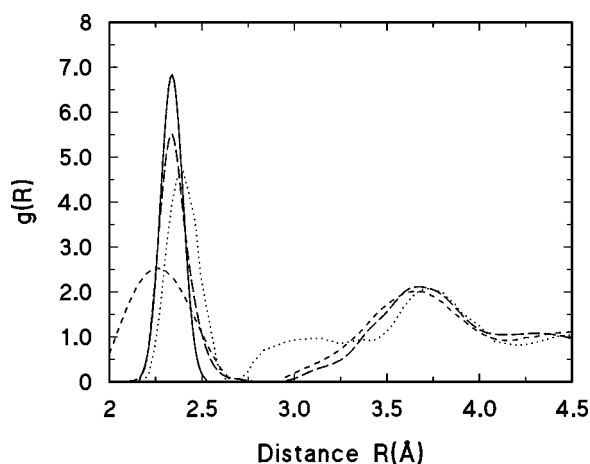


FIG. 14. A comparison of present XAFS pair-correlation function (first shell) of pure Se glasses at room temperature (full line) with the x-ray (Ref. 2) (long-dashed line) and neutron (Ref. 5) (short-dashed line) scattering experimental data at room temperature and with the molecular-dynamics simulation (Ref. 23) of amorphous (350 K) selenium (dotted line).

ture up to 0.0059 \AA^2 for the crystalline *t*-Te, while for the glasses the DW factor values increase only up to 0.0040 \AA^2 (see Table I).

Moreover, this contribution must be greater than the difference between the DW factors of the glasses and the reference crystals because we suggest that these bonds are stronger in glasses than in trigonal crystals. That can also explain why for the Te-Te₁ bond in the glasses the change of the DW factor values with temperature is smaller.

As we have noticed before, relatively little was known about the intrachain and interchain next nearest neighbors in the Se_{1-x}Te_x glasses, as the situation is sufficiently complicated in pure amorphous selenium, with strong overlap of intrachain and interchain contributions in the pair-correlation functions (see Fig. 14). Previous x-ray and neutron-scattering experiments^{1-5,23} on *a*-Se show above the first peak at 2.34 Å a smooth increase of amplitude above 3 Å up to the peak at 3.6–3.8 Å with the total (intrachain and interchain) coordination number at about 6–7 (see a summary of the data in Table I in Ref. 23). The *ab initio* molecular-dynamics study based on the local density approximation (LDA) of amorphous Se at 350 K shows the first sharp peak at 2.37 Å, the second broad peak at 2.8–3.5 Å, and the third peak at 3.6–3.8 Å. The results are in agreement with x-ray and neutron-scattering data, except in the region (2.8–3.5 Å) of interchain

next-nearest-neighbors contribution. The recent *ab initio* molecular-dynamics study with gradient correction to the LDA of liquid Se (570 K and higher temperatures) improves the agreement with scattering experiments, except in the region of the first minimum (2.9 Å).²⁴

Present XAFS measurements on the Se *K* edge are more sensitive than the previous x-ray and neutron-scattering experiments¹⁻⁵ because of the higher values of momentum transfer.

V. SUMMARY

Complementary XAFS measurements of Se_{1-x}Te_x glasses have been carried out on both the Se and Te *K* edges at low and room temperatures. XAFS analysis of experimental data is carried out on the first shell.

The reconstructed local intrachain order is in very close agreement with existing random chain models of glasses but reveal more information. There is very little MSRD in the nearest-neighbor intrachain distances, the thermal disorder dominates for Se-Se₁, Se-Te₁ (Te-Se₁), and Te-Te₁ pairs.

Detailed analysis of the distances in relation with the glassy composition shows that in the first coordination shell the distances present little elongation with Te content with the composition Se_{0.7}Te_{0.3}: the Se-Se₁ distance elongates from 2.340 Å to 2.347 Å, the Se-Te₁ (Te-Se₁) distance elongates from 2.540 Å to 2.545 Å, and the Te-Te₁ distance elongates from 2.725 Å to 2.740 Å. Then the distances suddenly increase with the composition Se_{0.6}Te_{0.4} up to 2.36 Å (Se-Se₁), 2.55 Å (Se-Te₁, Te-Se₁), and 2.745 Å (Te-Te₁).

From the first coordination shells results we conclude that the intrachain chemical order (preferential for Se-Te pairs) increases with Te content in the glasses. On the other hand, we suggest a random distribution of Se and Te atoms between the chains.

ACKNOWLEDGMENTS

M.M. and J.P. would like to thank Professor B. Legendre (Bioinorganique, Centre pharmaceutique Chatenay-Malabry, Université-Paris-Sud) for his great help during this work. Special thanks to the LURE and NSLS laboratories for the hospitality and support during our experiments. J.P. is indebted to Dr. A. Kuzmin, Professor G. Dalba, Professor P. Fornasini, and Professor F. Rocca for stimulating discussions of XAFS data analysis, and Professor Y. Mathey and Professor C. Bichara for helpful discussions.

*Electronic address: xas@acad.latnet.lv

¹E. H. Henninger, R. C. Buschert, and L. Heaton, *J. Chem. Phys.* **46**, 586 (1967).

²R. Kaplow, T. A. Rowe, and B. L. Averbach, *Phys. Rev.* **168**, 1068 (1968).

³R. Bellissent and G. Tourand, in *Proceedings of the 7th International Conference on Amorphous and Liquid Semiconductors*, edited by E. E. Owen and W. E. Spear (Stevenson, Dundee, 1977), p. 98.

⁴R. Bellissent and G. Tourand, *J. Non-Cryst. Solids* **35&36**, 1221 (1980).

⁵R. Bellissent, *Nucl. Instrum. Methods* **199**, 289 (1982).

⁶J. C. Malaurent and J. Dixmier, in *Proceedings of the Symposium on The Structure of Non-Crystalline Materials*, edited by P.H. Gaskell (Taylor & Francis, London, 1977), p. 49.

⁷T. M. Hayes and S. H. Hunter, in *Proceedings of the Symposium on the Structure of Non-Crystalline Materials* (Ref. 6), p. 69.

⁸K. Tamura, S. Hosokawa, H. Endo, S. Yamasaki, and H. Oyanagi, *J. Phys. Soc. Jpn.* **55**, 528 (1986).

⁹C. Y. Inui, M. Yao, and H. Endo, *J. Phys. Soc. Jpn.* **57**, 553 (1988).

¹⁰C. Y. Yang, D. E. Sayers, and M. A. Paesler, *J. Non-Cryst. Solids* **114**, 67 (1989).

¹¹K. Tamura, M. Inui, M. Yao, H. Endo, S. Hosokawa, H. Hoshino,

- Y. Katayama, and K. Maruyama, *J. Phys.: Condens. Matter* **3**, 7495 (1991).
- ¹²S. de Panfilis and A. Filippini, *Europhys. Lett.* **37**, 397 (1997).
- ¹³C. S. Kim and P. Boolchand, *Phys. Rev. B* **19**, 3187 (1979).
- ¹⁴G. Lucovsky, A. Mooradian, W. Taylor, G. B. Wright, and R. C. Keezer, *Solid State Commun.* **5**, 113 (1967).
- ¹⁵A. T. Ward, *J. Phys. Chem.* **74**, 4110 (1970).
- ¹⁶G. Lucovsky, in *The Physics of Selenium and Tellurium*, edited by E. Gerlach and P. Grosse (Springer, New York, 1979), p. 178.
- ¹⁷G. Lucovsky and C. K. Wong, *J. Non-Cryst. Solids* **75**, 51 (1985).
- ¹⁸G. Lucovsky and C. K. Wong, *Philos. Mag. B* **52**, 553 (1985).
- ¹⁹J. Robertson, *Philos. Mag.* **34**, 13 (1976).
- ²⁰F. Gompf, *J. Phys. Chem. Solids* **42**, 539 (1981).
- ²¹G. Carini, M. Cutroni, A. J. Dianoux, G. Galli, L. M. Needham, and H. M. Rosenberg, *J. Non-Cryst. Solids* **117**, 140 (1990).
- ²²W. A. Phillips, U. Buchenau, N. Nücker, A.-J. Dianoux, and W. Petry, *Phys. Rev. Lett.* **63**, 2381 (1989).
- ²³D. Hohl and R. O. Jones, *Phys. Rev. B* **43**, 3856 (1991).
- ²⁴F. Kirchoff, M. J. Gillan, J. M. Holender, G. Kresse, and J. Hafner, *J. Phys.: Condens. Matter* **8**, 9353 (1996).
- ²⁵C. Bichara, J.-Y. Raty, and J.-P. Gaspard, *Phys. Rev. B* **53**, 206 (1996).
- ²⁶P. Unger and P. Cherin, in *The Physics of Selenium and Tellurium*, edited by W. C. Cooper (Pergamon Press, London, 1969), p. 223.
- ²⁷J. B. Parise, J. E. MacDougall, N. Herron, R. Farlee, A. W. Sleight, Y. Wang, T. Bein, K. Moller, and L. Moroney, *Inorg. Chem.* **27**, 220 (1988).
- ²⁸G. Ghosh, R. S. Sharma, D. T. Li, and Y. A. Chang, *J. Phase Equilib.* **15**, 213 (1994).
- ²⁹M. F. Kotkata, E. A. Mohmoud, and M. K. El-Mously, *Acta Phys. Acad. Sci. Hung.* **50**, 61 (1981).
- ³⁰H. Watanabe and K. C. Rao, *Jpn. J. Appl. Phys.* **18**, 1849 (1979).
- ³¹R. C. Keezer and M. W. Bailey, *Mater. Res. Bull.* **2**, 158 (1967).
- ³²W. W. Warren, Jr. and R. Dupree, *Phys. Rev. B* **22**, 2257 (1980).
- ³³Th. Koslowski and W. von Niessen, *Phys. Rev. B* **49**, 11 704 (1994).
- ³⁴Th. Koslowski, *J. Phys.: Condens. Matter* **9**, 613 (1997).
- ³⁵R. B. Stephens, *Phys. Rev. B* **30**, 5195 (1984).
- ³⁶J. Robertson, *Philos. Mag. B* **51**, 183 (1985).
- ³⁷R. Steudel, *J. Non-Cryst. Solids* **83**, 63 (1986).
- ³⁸J. Moscinski, A. Renninger, and B. L. Averbach, *Phys. Lett.* **42A**, 453 (1973).
- ³⁹H. Thurn and J. Ruska, *J. Non-Cryst. Solids* **22**, 331 (1976).
- ⁴⁰K. Matsuishi, H. Kasamura, S. Onari, and T. Arai, *J. Non-Cryst. Solids* **114**, 46 (1989).
- ⁴¹Y. Tsuchiya, *J. Phys.: Condens. Matter* **20**, 1209 (1987).
- ⁴²G. Morgant and B. Legendre, *J. Therm. Anal.* **31**, 377 (1986).
- ⁴³A. Amzil, M. Gilbert, C. Bichara, and J.-C. Mathieu, *J. Phys.: Condens. Matter* **8**, 5281 (1996).
- ⁴⁴A. Kuzmin, *Physica B* **208&209**, 175 (1995); *J. Phys. IV* **7**, C2-213 (1997).
- ⁴⁵A. Kuzmin and J. Purans, *J. Phys.: Condens. Matter* **5**, 2333 (1993); A. Kuzmin, N. Mironova, J. Purans, and A. Rodionov, *ibid.* **7**, 9357 (1995).
- ⁴⁶F. Rocca, A. Kuzmin, J. Purans, and G. Mariotto, *Phys. Rev. B* **50**, 6662 (1994).
- ⁴⁷Q. Ma, D. Raoux, and S. Bénazeth, *Phys. Rev. B* **48**, 16 332 (1993).
- ⁴⁸A. G. MaKale, B. W. Vael, A. P. Pauliklas, S.-K. Chan, and G. S. Knapp, *J. Am. Chem. Soc.* **110**, 3763 (1988).
- ⁴⁹J. J. Rehr, J. Mustre de Leon, S. I. Zabinsky, and R. C. Albers, *J. Am. Chem. Soc.* **113**, 5135 (1991); J. Mustre de Leon, J. J. Rehr, S. I. Zabinsky, and R. C. Albers, *Phys. Rev. B* **44**, 4146 (1991).
- ⁵⁰M. Majid, S. Bénazeth, C. Souleau, and J. Purans, *J. Phys. IV* **7**, C2-999 (1997).
- ⁵¹Y. Mathey, H. Sassoli, and J. Purans, *J. Alloys Compd.* **262-263**, 81 (1997).
- ⁵²M. C. Co and K. O. Hodgson, *J. Am. Chem. Soc.* **103**, 3200 (1981).
- ⁵³N. Binsted, R. W. Strange, and S. S. Hasnain, *Biochemistry* **31**, 12 117 (1992).
- ⁵⁴W. L. Schaich, *Phys. Rev. B* **14**, 4420 (1976).
- ⁵⁵S. J. Gurman, N. Binsted, and I. Ross, *J. Phys. C* **17**, 143 (1984).
- ⁵⁶E. A. Stern and S. M. Heald, in *Handbook of Synchrotron Radiation*, edited by B. E. Kock (North-Holland, Amsterdam, 1983), Vol. 1B, Chap. 10.
- ⁵⁷G. Bunker, *Nucl. Instrum. Methods Phys. Res.* **207**, 437 (1983).
- ⁵⁸G. Dalba, P. Fornasini, and F. Rocca, *Phys. Rev. B* **47**, 8502 (1993).
- ⁵⁹G. Dalba, P. Fornasini, M. Grazioli, and F. Rocca, *Phys. Rev. B* **52**, 11 034 (1995).
- ⁶⁰E. Stern, *Jpn. J. Appl. Phys., Part 1* **32**, 851 (1993).
- ⁶¹A. Filippini and A. DiCiccio, *Phys. Rev. B* **51**, 12 322 (1995).
- ⁶²*X-Ray Absorption Fine Structure*, edited by S. S. Hasnain (Ellis Horwood, New York, 1991), p. 751.
- ⁶³G. G. Li, F. Bridges, and C. H. Booth, *Phys. Rev. B* **52**, 6332 (1995).
- ⁶⁴R. W. Joyner, K. J. Martin, and P. Meehan, *J. Phys. C* **20**, 4005 (1987).
- ⁶⁵P. Boolchand and P. Suranyi, *Phys. Rev. B* **7**, 57 (1973).
- ⁶⁶A. F. Wells, *Structural Inorganic Chemistry* (Oxford University Press, New York, 1984), p. 699.
- ⁶⁷Y. Ohmasa, I. Yamamoto, M. Yao, and H. Endo, *J. Phys. Soc. Jpn.* **64**, 4766 (1995).
- ⁶⁸A. Ikawa, *J. Phys. Soc. Jpn.* **66**, 676 (1997).
- ⁶⁹R. Keller, W. B. Holzapfel, and H. Schulz, *Phys. Rev. B* **16**, 4404 (1977).
- ⁷⁰A. Ikawa and H. Fukutome, *J. Non-Cryst. Solids* **117&118**, 328 (1990).
- ⁷¹H. Sakai, M. Yao, M. Inui, K. Maruyama, K. Takimoto, and H. Endo, *J. Phys. Soc. Jpn.* **57**, 3587 (1988).